RESEARCH ARTICLE

Efficient degradation of microcystin-LR by BiVO$_4$/TiO$_2$ photocatalytic nanocomposite under visible light

Negar Jafari[1] · Karim Ebrahimpour[2,3] · Ali Abdolahnejad[2,3] · Mahbobe Karimi[4] · Afshin Ebrahimi[2,3]

Abstract

Microcystin-Leucine Arginine (MC-LR) is one of the most studied cyanotoxins due to its toxicity and abundant that cause health hazards for humans through of the drinking water. In this study, BiVO$_4$/TiO$_2$ nanocomposite was synthesized by hydrothermal method and employed for the removal of MC-LR. The characteristics of the catalysts were determined by FESEM, XRD and FTIR spectra. Response surface methodology (RSM) was applied to assess the effects of operating variables (pH, contact time, and catalyst dose) on the MC-LR removal. The coefficient of determination (R^2) was calculated 98.7% for the response. The residual concentration of MC-LR was measured by high-performance liquid chromatography (HPLC). The results show that the highest removal efficiency of MC-LR was 98% under the optimum conditions (pH = 5, contact time = 90 min, and catalyst dose = 0.5 g/l). MC-LR decomposition efficiency by BiVO$_4$/TiO$_2$ nanocomposite was enhanced by pH reduction and increasing of contact time and catalyst dose. The prepared BiVO$_4$/TiO$_2$ nanocomposite with technological potential can be used directly in environmental preservation, specifically in the decontamination of MC-LR from aqueous solutions.

Keywords Microcystin-LR degradation · BiVO$_4$/TiO$_2$ nanocomposite · Photocatalysis · Visible light

Introduction

Microcystins (MCs) are potent hepatotoxins produced by cyanobacteria which can cause a significant health hazard in drinking water [1–3]. Among the various MCs, Microcystin-leucine-arginine (MC-LR) is the most common of the microcystins due to its toxicity and abundant in environment [3, 4]. Moreover, the World Health Organization (WHO) is recommended a limit of 1 μg/L for total MC-LR for water for human consumptions [5]. When MCs ingest orally absorb to hepatocytes and prohibit protein phosphatase, subsequently resulted in cell structures disruption, intrahepatic hemorrhage, and death [6, 7]. In 1996 MC-LR was responsible for the death of 52 Brazilian kidney dialysis patients [8]. Various techniques have suggested for the cyanobacteria cells and MCs control in drinking water, such as coagulation, flocculation, filtration, activated carbon, membrane filtration, oxidation processes and etc. [9, 10]. For example, use of the enhanced coagulation-sediment-filtration to simultaneously remove algal cells and their metabolites is economical [11]. But conventional water treatment, only can be effective for the removal of microcystin intracellular while extra cellular toxin remained after flocculation and filtration [12]. PAC effectively removes MCs from water up to 99% but PAC is effectively adsorbed extracellular MCs and not removed the intracellular MCs [13, 14]. MF and UF techniques are not expected to remove extracellular MC and require costly pumping of water as well as face fouling and cell lysis problems. MC-LR was reduced more than 95% by NF and RO membranes but they require

✉ Afshin Ebrahimi
a_ebrahimi@hlth.mui.ac.ir

Negar Jafari
n64jafari@gmail.com

Karim Ebrahimpour
k.ebrahiim@gmail.com

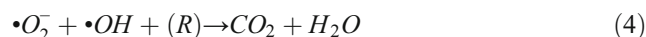1 Student Research Committee, School of Health, Isfahan University of Medical Sciences, Isfahan, Iran

2 Environment Research Center, Research Institute for Primordial Prevention of Non-communicable disease, Isfahan University of Medical Sciences, Isfahan, Iran

3 Department of Environmental Health Engineering, School of Health, Isfahan University of Medical Sciences, Isfahan, Iran

4 Department of Chemistry, University of Isfahan, Isfahan, Iran

a high cost and high technique level of maintenance to prevent membrane fouling by NOM and cyanobacterial cells [13]. Ozone is the most effective agent for the destruction of intracellular and extracellular cyanotoxin but its ability for MCs removal depends on pH, so that about neutral pH, oxidation of MCs will be may not achieve desired removal [15–17].Recently, in order to remove these toxins in raw waters, more studies have focused on the application of advanced oxidation processes (AOPs) such as UV/H_2O_2 [18], Fenton regents [19, 20], and photocatalysis [21]. In advanced oxidation processes are generated •OH, •O, and •HO_2 species that considerably promised for the decomposition of MCs [22–24]. Photocatalysts have been examined for the organic and inorganic pollutants degradation [25]. Among them, semiconductor nanostructures with superior optical and physicochemical characteristics are used for environmental applications. TiO_2 is one of the semiconductor photocatalysts that because of its chemical stability, chemical inertness, non-toxicity, low cost, and strong oxidizing ability is most interested [26–29], but despite of its desirable properties, because to having of large band gap (~3.2 eV) activates only in the UV light region [30, 31]. Therefore, the formation of heterojunction structures between TiO_2 and a narrow band gap semiconductor such as Bismuth vanadate ($BiVO_4$) can efficiently extend the photosensitivity of TiO_2 into the visible region [32]. $BiVO_4$ is a low-cost semiconductor that has attracted special great attention for the organic pollutants degradation [33, 34]. TiO_2 coupled by $BiVO_4$ is alternated as a way for enhancement of photocatalytic performance [35]. Absorption of a photon by semiconductors excites an electron from the valence band (VB) to the conduction band (CB), if the photon energy [36] equals or exceeds from the semiconductor/photocatalyst band gap [20]. Simultaneously, a positive charge called a hole (h^+) is also generated in the VB and resulted inthe formation of electron-hole pairs (Eq. (1)) [25]. Then these pairs ($e^-–h^+$ pair) move to the photocatalyst surface and in redox reactions with the adsorbed pollutants on the photocatalyst recombines, producing thermal energy or participate. The lifetime of an $e^-–h^+$ pair is very low [37] but is still enough for the promotion of redox reactions in the solution or gas phase in the semiconductor surface [25]. Then the photo-excited electrons react with molecular oxygen (O_2) to the production of superoxide radical anions (•O_2^-) [38] (Eq. (2)), and the photo generated holes react with water to produce hydroxyl radicals (•OH) (Eq. (3)). Therefore, nanocomposites are enabled to have a powerful and durable photooxidation capability through generation of these strong radicals [39].As these radicals are the main active species in the photo-oxidation process under visible light [40], they play crucial roles in the decomposition of the toxic and persistent organic pollutants (R) present at the surface of the photocatalyst and convert them into harmless species. The products due to the photodegradation are reduced to mineral compounds and finally CO_2 and H_2O are released (Eq. (4)) [41].

$$Photocatalyst \xrightarrow{h\nu} e^- + h^+ \tag{1}$$

$$e^- + O_2 \rightarrow \bullet O_2^- \tag{2}$$

$$h^+ + OH^- \rightarrow \bullet OH \tag{3}$$

$$\bullet O_2^- + \bullet OH + (R) \rightarrow CO_2 + H_2O \tag{4}$$

This study was performed with the aim to degradation of microcystin-LR by $BiVO_4$/TiO_2 nanocomposite by Response Surface Methodology (RSM) based on Central Composite Design (CCD) to optimize the performance of nanocomposites with consideration of effective variables on process efficiency. This prepared nanocomposites already was used for some organic pollutants removal but up to date there was not seen a study that uses this nanocomposite for MC-LR removal.
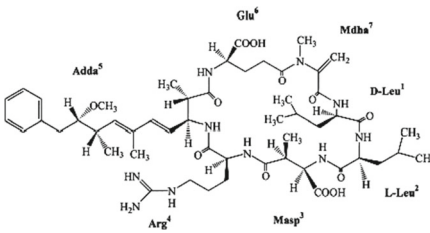
Experimental

Materials

MC-LR standard solution (10 μg/mL) was purchased from Sigma-Aldrich Co. (USA). In addition, MC-LR standard powder (100 μg) also was purchased from Enzo Life Sciences, Inc., USA. Then the solutions were prepared by dissolving the standard powder in 100% methanol (1 mL) before diluting to working solutions using high-purity water (Merck, Germany). All standards and the working solutions were stored at −20 °C until use. The MC-LR physicochemical properties such as molecular structure and weight (g/mol), chemical formula and solubility in water and density are demonstrated in Table 1 $Bi(NO_3)_3.5H_2O$ (bismuth nitrate), NH_4VO_3 (ammonium metavanadate) and TiO_2 (anatase, purity: 99.9 wt%, particle size: 20 nm, and BET>200 m^2/g) were purchased from Sigma-Aldrich Co. (USA). High-performance liquid chromatography (HPLC)-grade methanol, acetonitrile, and trifluoroacetic acid (TFA) were provided by Merck (Germany).

Preparation of $BiVO_4$/TiO_2 nanocomposite

$BiVO_4$/TiO_2 nanocomposite was synthesized by hydrothermal method. Briefly, 0.02 mol of $Bi(NO_3)_3.5H_2O$ and 0.02 mol of NH_4VO_3 were dissolved in 20 mL of 4 M HNO_3 and 2 M NaOH aqueous solutions, respectively, to form two transparent solutions. These solutions were mixed together with Bi:V molar ratio of 1:1. The orange slurry was obtained by adjusting pH to 7 with 4 M NaOH. Then an appropriate amount of TiO_2 powder was subsequently added to the pre-prepared $BiVO_4$ solution (50:50 W/W ratio) and

Table 1 Physicochemical properties of MC-LR [42]

Physicochemical properties	MC-LR
Molecular structure	[42]
Molecular weight (g/mol)	995
Chemical formula	$C_{49}H_{74}N_{10}O_{12}$
Solubility in water (g/l)	>1
Density (g/cm^3)	1.299

was stirred for 2 h under ambient air. After this time, the suspension was transferred into a Teflon-lined stainless steel autoclave with a capacity of 100 mL and the hydrothermal reaction was carried out at 180 °C for 24 h, and then cooled down to room temperature. The final product was filtered and washed with deionized water several times and then was dried at 80 °C for several hours. Finally, the resultant sample was calcined at 500 °C for 6 h. Furthermore, the pure $BiVO_4$ was prepared without the addition of TiO_2 powder and was used to the next experiments [43].

Characterization of nanocomposite

Field emission scanning electron microscope (FESEM) (FEI Quanta 200, USA) was used to investigate the $BiVO_4$ and TiO_2nanoparticles and $BiVO_4/TiO_2$nanocomposite structure and surface morphology. The crystalline nature was also revealed by X-ray diffractometer (XRD, Bruker D8 Advance, Germany).FTIR spectrum of $BiVO_4/TiO_2$ was recorded using an IR spectrometer (Jasco 6300, Japan).

Photocatalytic setup

All of the experiments were performed in 25 mL Pyrex beakers involving 10 mL of aquatic solutions with 500 μg/L MC-LR concentration and catalyst mixture. The pH of the samples was adjusted by 0.01 M NaOH and HCl. Then, the samples were put in an ultrasonic bath for 10 min to eliminate aggregates. Photocatalyst suspensions were illuminated with 15 W LED lamps (white light). These lamps were located in 10 cm above beakers. Firstly, the samples were stirred for 30 min to reach equilibrium in darkness. Then, lamps were turned on and samples were placed under magnetic stirring to maintaining agitation during the reaction to keep suspension uniformity. At the end of contact time, lamps were turned off and samples were taken and filtrated through 0.22 μm syringe filters to separate the catalyst particles before measuring the residual MC-LR content by HPLC.

Design of Experiment: RSM approach

Response surface methodology (RSM) was used for the experimental design by Design Expert software 10 by using central composite design (CCD) as a most widely used method to evaluate the interactive effects of the significant operating parameters and to optimize the MC-LR degradation by $BiVO_4/TiO_2$ photocatalytic nanocomposite [44]. The three main parameters pH (A), contact time (B), and catalyst dose (C) were chosen as model variables to study their interaction effects on the ability of $BiVO_4/TiO_2$ nanocomposite for MC-LR removal. Also, the each of $BiVO_4$ and TiO_2 nanoparticles only were tested under specified terms by Design Expert software 10. In general, a central composite design (CCD) in RSM software consists of 2^k points that form the base design, 2 k axial points (star points) and several center points, where k is the number of variables [45].Each independent actual parameter was varied over three coded values (−1, 0, +1), which composed the batch experimental design matrix derived from the CCD summarized in Table 2.

Table 2 Actual and coded values of independent variables for the CCD used in this study

Variables (unit)	Symbol	Coded level		
		−1	0	+1
pH	A	5	7	9
Contact time (min)	B	30	60	90
Catalyst dose (g/l)	C	0.2	0.35	0.5

Overall 20 different experimental runs (including six replicates of the center point for error evaluation and 8 full factorial (the base design) were designed, along with the predicted and actual MC-LR removal values are shown in Table 3.

The coded values of independent variables were calculated based on Eq. (5):

$$Xi = \frac{(Xi - X0)}{\Delta X} \tag{5}$$

where Xi is a coded value of the independent variable, X0 is the center point value and ΔX is the change value [36]. These numbers of runs were employed to investigate the interaction between the independent and the dependent variables through following regression model (Eq. (6)):

$$Y = \beta_0 + \sum \beta_i X_i + \sum \beta_{ii} X_i^2 + \sum \beta_{ij} X_i X_j \tag{6}$$

Where Y is the predicted response of MC-LR removal (response), β_0 is the model constant, βi is the linear coefficient, βii is the quadratic coefficient and the βij is the cross product coefficient.

MC-LR quantification

The concentration of MC-LR in the samples was determined by an HPLC system (Jasco PU-2080, Tokyo, Japan) which was equipped with a quaternary mixing pump, an inline vacuum degasser, automatic injector (AS-2055 Plus), a C_{18} column (150 × 4.6 mm, Germany), packed with 5 μm particles for the separation, and an UV-Vis detector (UV-2075 plus). The used mobile phase was a gradient of Mili-Q water and acetonitrile (50:50, v/v), both with 0.1% of TFA. Wavelength was set at 238 nm to the typical absorption spectra of MC-LR. The injection volume was 100 μl with a flow rate of 1 mL/min. Total run time was 15 min. Data acquisition and processing were done using BORWIN Chromatography software (Version 1.50). The degradation rate of MC-LR was calculated by the (Eq. (7)):

$$Degradation\,(\%) = \frac{C_0 - C}{C_0} \times 100 \tag{7}$$

Where C_0 and C are the initial and the residual concentrations of MC-LR.

Table 3 Experimental conditions & results of central composite design (CCD)

Run. No	Variables			MC-LR removal (%)	
	A pH	B Contact time(min)	C Catalyst dose(g/l)	Actual	Predicted
1	9	90	0.5	88.23	88.64
2	7	60	0.35	71.29	72.35
3	7	60	0.12	80.21	82.39
4	7	60	0.35	72.59	72.35
5	9	90	0.2	83.76	82.54
6	5	30	0.5	91.86	92.34
7	9	30	0.5	75.37	74.94
8	7	14.3	0.35	71.41	72.55
9	7	60	0.35	73.98	72.35
10	4	60	0.35	83.54	83.58
11	5	90	0.5	97.97	98.39
12	7	60	0.35	74.01	72.35
13	7	60	0.35	70.89	72.35
14	9	30	0.2	69.45	68.29
15	5	30	0.2	81.93	80.78
16	5	90	0.2	87.7	87.39
17	7	105.7	0.35	87.9	88.03
18	7	60	0.35	72.19	72.35
19	7	60	0.58	96.76	95.85
20	10	60	0.35	65.39	66.62

Validation of the method

The validation of the analytical method was done according to International Conference on Harmonization (ICH) recommendations for relative standard deviation (RSD), relative recovery, limit of detection (LOD), and limit of quantification (LOQ), (Table 4).

Results and discussions

Catalysts characterization

Field emission scanning electron microscope (FESEM) graphs of the studied photocatalysts are presented in Fig. 1. It can be shown that symmetric spherical nanoparticles of BiVO₄ (Fig. 1a), and angled asymmetric TiO₂ nanoparticles (Fig. 1b) were synthesized to form BiVO₄/TiO₂ nanocomposite (Fig. 1c). Therefore, the obtained nanocomposite has very different structure and more porous surface than its ingredients.

For each of pristine BiVO₄, and TiO₂ nanoparticles; and BiVO₄/TiO₂ nanocomposite, separately, X-ray diffraction (XRD) patterns were measured using an X-ray diffractometer at 40 kV and 40 mA with Ni-filtered Cu Kα radiation (λ = 0.15406 nm) at a scan rate of 1°/min in 2θ ranging from 5° to 80° (Fig. 2). The crystallite size was estimated using the Debye-Scherrer formula (Eq. (8)):

$$D = K\lambda/(\beta cos\ \theta) \tag{8}$$

where D is the crystallite size, λ is the wavelength of the X-ray radiation, K is a constant taken as 0.89, β is the full width at half maximum corresponding to the Bragg's angle θ. Therefore, based on XRD, the average crystal sizes of BiVO₄ and TiO₂ in synthesized nanocomposite were 35 and 20 nm, respectively.

As can be seen, the crystal phase of anatase TiO₂ nanoparticles is included in the diffraction peaks at about 2θ = 25.33°, 37.8°, 48.1°, 53.9° and 55.1° (PDF number 21–1272, JCPDS). Also, all of the peaks match well to the monoclinic scheelite BiVO₄ with the diffraction peaks at about 2θ = 18.99°, 28.95°, 30.57°, 39.87°, and 53.22° (PDF number 14–0688, JCPDS). Moreover, there is no any other phase or impurity peak in the resulted XRD pattern (Fig. 2), which

confirms that the synthesized BiVO₄/TiO₂ nanocomposite sample by the hydrothermal method has high purity and is only composed of monoclinic BiVO₄ and TiO₂ nanoparticles.

Figure 3 shows the FTIR spectra of BiVO₄ and TiO₂ nanoparticles; and BiVO₄/TiO₂ nanocomposite. According to this Figure, in the FTIR spectra of BiVO₄, the wavelength of 730 cm^{-1}, was associated with the V-O-V band that indicating the asymmetric stretching vibration. The region of 480–410 cm^{-1} was assigned to symmetry bending, namely oxygen bonds with bismuth (Bi-O) and vanadium metals (V-O). In the FTIR spectra of TiO₂, index peaks of 3408 cm^{-1} and 1632 cm^{-1}, refers to stretching vibrations of hydroxyl groups (O-H bonds). and bending vibrations of adsorbed water molecules on its surface, respectively. The broad intense bond between 1000 and 400 cm^{-1} has been related to Ti-O-Ti vibration [44, 46].

Finally, in the FTIR spectra of BiVO₄/TiO₂ nanocomposite, the band at 3432 cm-1was attributed to O-H stretching vibration on composite. The adsorption band at 1624 cm^{-1}also was related to Ti-O-H bending mode on the surface of the synthesized sample. The region of 730–470 cm^{-1} was due to the chemical or structural effects of the Bi^{3+} or VOx ion in BiVO₄/TiO₂ nanocomposite lattice, demonstrating an interconnection between BiVO₄ and TiO₂.

Statistical analysis

The analysis of variance (ANOVA) was carried out based on the suggested model to show the interaction among three variables (pH, contact time, and catalyst dose) and MC-LR degradation as the response parameters. In addition, the coefficient of determination (R^2), adjusted R^2 (R$^2_{adj}$), p value, and F-value which show the goodness of fit of the obtained regression model are summarized in Table 5.

According to this Table, the model F-value of 85.58 implies that the model is significant. In addition, the values of "Prob>F" less than 0.05 indicate model terms are significant. On the other hand, A, B, C, AB, AC, A^2, B^2, and C^2 symbols are significant model terms. However, the values greater than 0.05 indicate the model terms are not significant. For example, the BC symbol is not significant. The Lack of Fit F-value = 1.57 implies the lack of fit is not significant relative to the pure error. The non-significant lack of fit value for the fitting model (p value>0.05) suggests that the quadratic model is valid for

Table 4 Method validation parameters for determination of MC-LR by HPLC

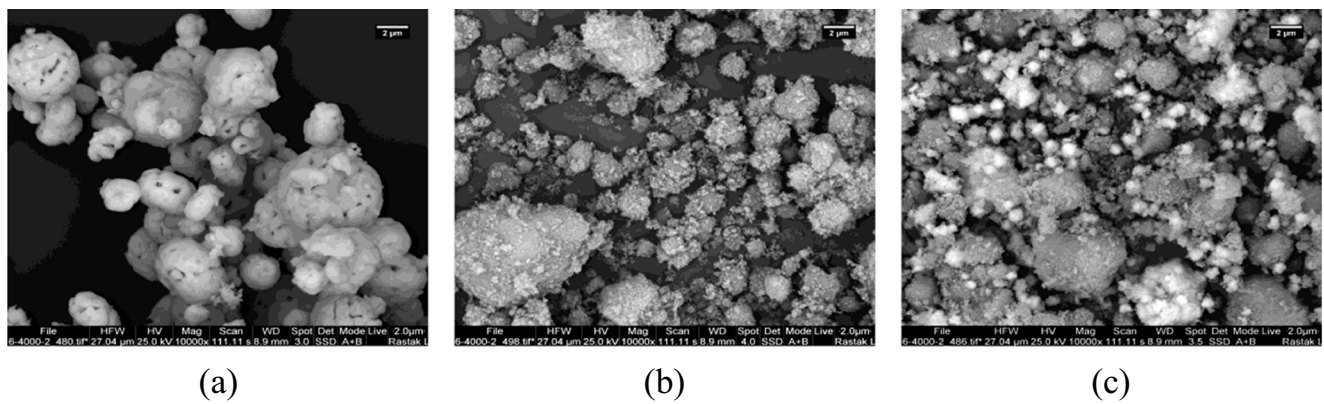| Parameter	RSD (%) (n = 5)		Recovery (%)	LOD (μg/L)	LOQ (μg/L)
	Within days	Between days			
MC-LR	5.19	4.22	102 ± 9.5	4.04	12.24

Fig. 1 FESEM images of a) $BiVO_4$;b) TiO_2 nanoparticles;and c) $BiVO_4/TiO_2$ nanocomposite

this process and errors of experiments are low. This relation shows that the model is significant.

Model fitting

To study the combined effect of all the variables, experiments were performed with different combinations of the variables, which were statistically designed by using CCD. The following equation represents the first model that was developed with all linear, two-way, and quadratic interaction of predictors:

$$Y = 72.35 – 5.56 \ A + 5.07 \ B + 4.41 \ C$$
$$+ 1.91 \ AB – 1.23 \ AC – 0.14 \ BC + 1.18 \ A^2$$
$$+ 3.42 \ B^2 + 7.22 \ C^2 \qquad (9)$$

The predicted R^2 of this preliminary model was 0.9341. To achieve a final model with significant predictors, the only not

significant interaction, BC: (p value = 0.8), was removed from this model. Thus, all of the other variables were significant and retained in the final regression model. Table 6 shows the final regression model variables for MC-LR removal.

The final equation was derived using the coefficient of the coded variables for MC-LR degradation as follow (Eq. 10):

$$MC−LR \ degradation \ (\%) = 72.35 – 5.56 \ A + 5.07 \ B$$
$$+ 4.41 \ C$$
$$+ 1.91 \ AB – 1.23 \ AC$$
$$+ 1.18 \ A^2 + 3.42 \ B^2$$
$$+ 7.22 \ C^2 \qquad (10)$$

This equation has relatively higher fitness (the lack of fit F-value = 1.32) and confirms a proper fit of this model. Also, the other coefficients and factors were improved in order to the model fitness. The correlation between the actual and

Fig. 2 XRD patterns of a) $BiVO_4$;b) TiO_2 nanoparticles;and c) $BiVO_4/TiO_2$ nanocomposite

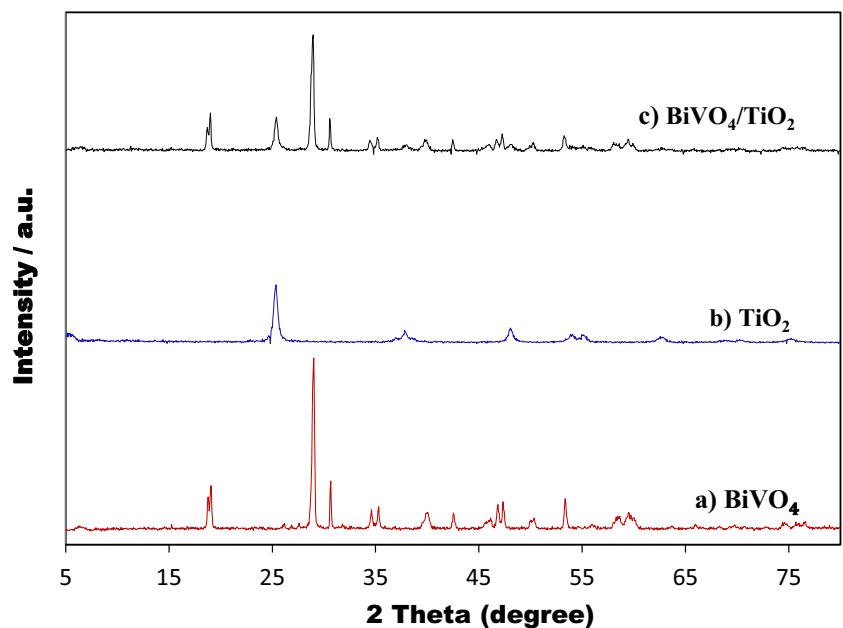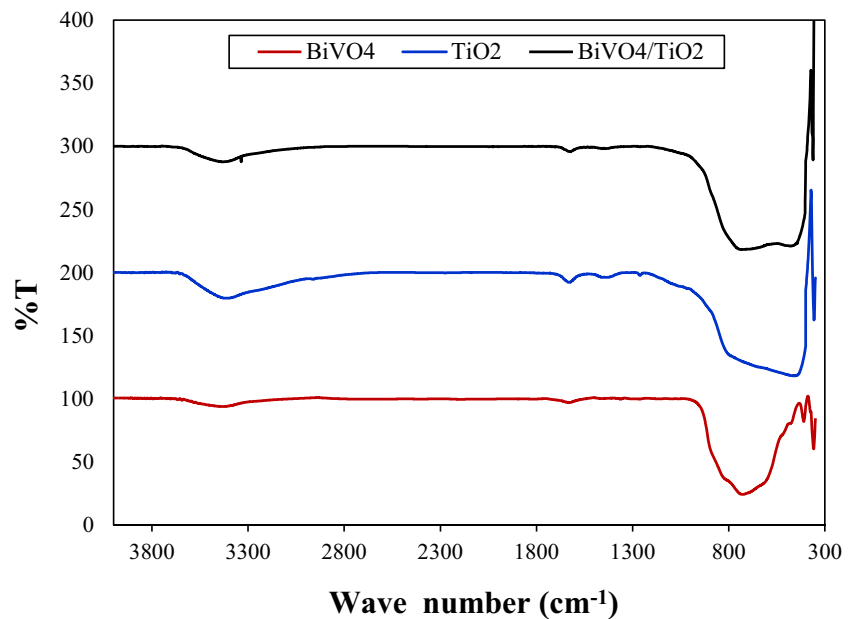**Fig. 3** FTIR spectra of BiVO$_4$; TiO$_2$ nanoparticles; and BiVO$_4$/TiO$_2$ nanocomposite

predicted MC-LR removal efficiencies and the normal plot of residual related to experimental data are shown in Fig. 4a and b, respectively.

According to these figures, the data points were well distributed close to a straight line, which indicated an excellent relationship between the experimental and predicted values of the response for BiVO$_4$/TiO$_2$ nanocomposite. These results also demonstrated that the chosen model was appropriate in assuming the response variables for the experimental data.

Effect of variables on photocatalytic degradation of MC-LR

Single variables

According to Table 5, between the single variables (pH, contact time, and catalyst dose), each factor that poses the highest mean square and F-value has the most effect in the degradation of MC-LR. Therefore, pH was the most important

Table 5 ANOVA results for response surface quadratic model

Source	Sum of Squares	df	Mean Square	F Value	p value Prob > F
Model	1708.39	9	189.82	85.58	<0.0001
A-pH	390.96	1	390.96	176.25	<0.0001
B-Contact time	325.76	1	325.76	146.86	<0.0001
C-Catalyst dose	246.36	1	246.36	111.06	<0.0001
AB	29.22	1	29.22	13.17	0.0046
AC	12.03	1	12.03	5.42	0.0421
BC	0.15	1	0.15	0.069	0.7975[*]
A^2	15.15	1	15.15	6.83	0.0259
B^2	126.16	1	126.16	56.87	<0.0001
C^2	562.61	1	562.61	253.64	<0.0001
Residual	22.18	10	2.22		
Lack of Fit	13.55	5	2.71	1.57	0.3163[*]
Pure Error	8.63	5	1.73		
Cor. Total	1730.57	19			

Std. Dev.: 1.49; Mean: 79.82; C.V. %: 1.87; PRESS: 113.97; R^2: 0.9872; Adj R^2: 0.9756; Pred R^2: 0.9341;

Adeq. Precision: 30.161.

*not significant

Table 6   Final regression model variables for MC-LR removal

Factor	Coefficient Estimate	df	Standard Error	95% CI	
				Low	High
Intercept	72.35	1	0.57	71.09	73.61
A-pH	−5.56	1	0.40	−6.44	−4.68
B-Contact time	5.07	1	0.40	4.19	5.96
C-Catalyst dose	4.41	1	0.40	3.53	5.30
AB	1.91	1	0.50	0.80	3.02
AC	−1.23	1	0.50	−2.34	−0.12
A^2	1.18	1	0.43	0.23	2.14
B^2	3.42	1	0.43	2.46	4.37
C^2	7.22	1	0.43	6.26	8.17

Std. Dev.: 1.42; Mean: 79.82; C.V. %: 1.79; PRESS: 87.09; R^2: 0.9871; Adj. R^2: 0.9777;

Pred. R^2: 0.9497; Adeq. Precision: 33.374.

parameter (mean square and F-value were equal 390.96 and 176.25, respectively). Also, pH parameter has a negative effect on MC-LR removal (negative sign in (Eq. (10)). The contact time and catalyst dose parameters have lower importance than pH. Of course, both have a positive effect on MC-LR removal (positive sign in (Eq. (10)).

Effect of pH

As mentioned earlier, the pH variable has a negative effect in MC-LR removal. Namely, the removal efficiency of MC-LR is increased with decreasing pH in the range of 5 to 9 (Fig. 5A).

The pH is an important factor in the organic pollutants photocatalytic removal from aqueous solutions [47]. This parameter may affect on the photocatalyst surface charge and also the state of ionization of the substrate [48] and hence its photo-degradation. In photocatalytic systems, the optimal pH was determined in the acidic range, which strong electrostatic adsorption could happen between the positively charged catalyst and the negatively charged toxin [49]. In the photocatalytic degradation of Acid Blue 113 and Acid Red 88 textile dyes, increasing pH decreased efficiency. Because acidic pH could affect the speciation of dye molecules and consequently, the electrostatic force between catalysts particles and dye molecules [50]. Similar results reported by Rahimi et al., that the acid orange 10 dye degradation efficiency was increased in the acidic pH [51].

The main reasons for the better MC-LR removal in acidic pH are:

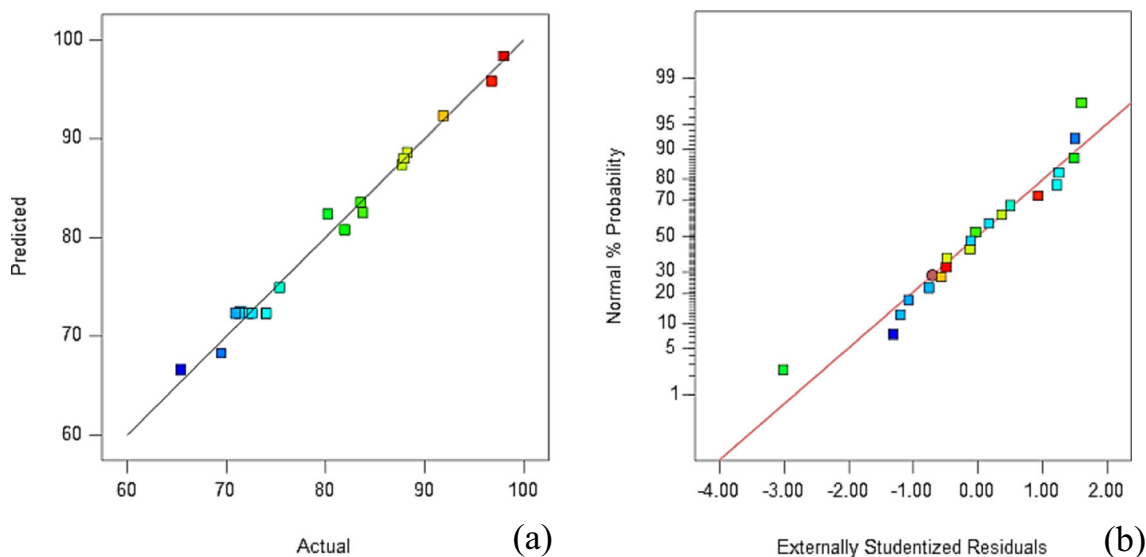1) The tendency of MC-LR molecule to wrapping and reducing molecular dimensions and hydrogen bonds

Fig. 4 (a) Correlation of actual versus predicted MC-LR removal efficiencies; (b) Normal plot of residual related to experimental data
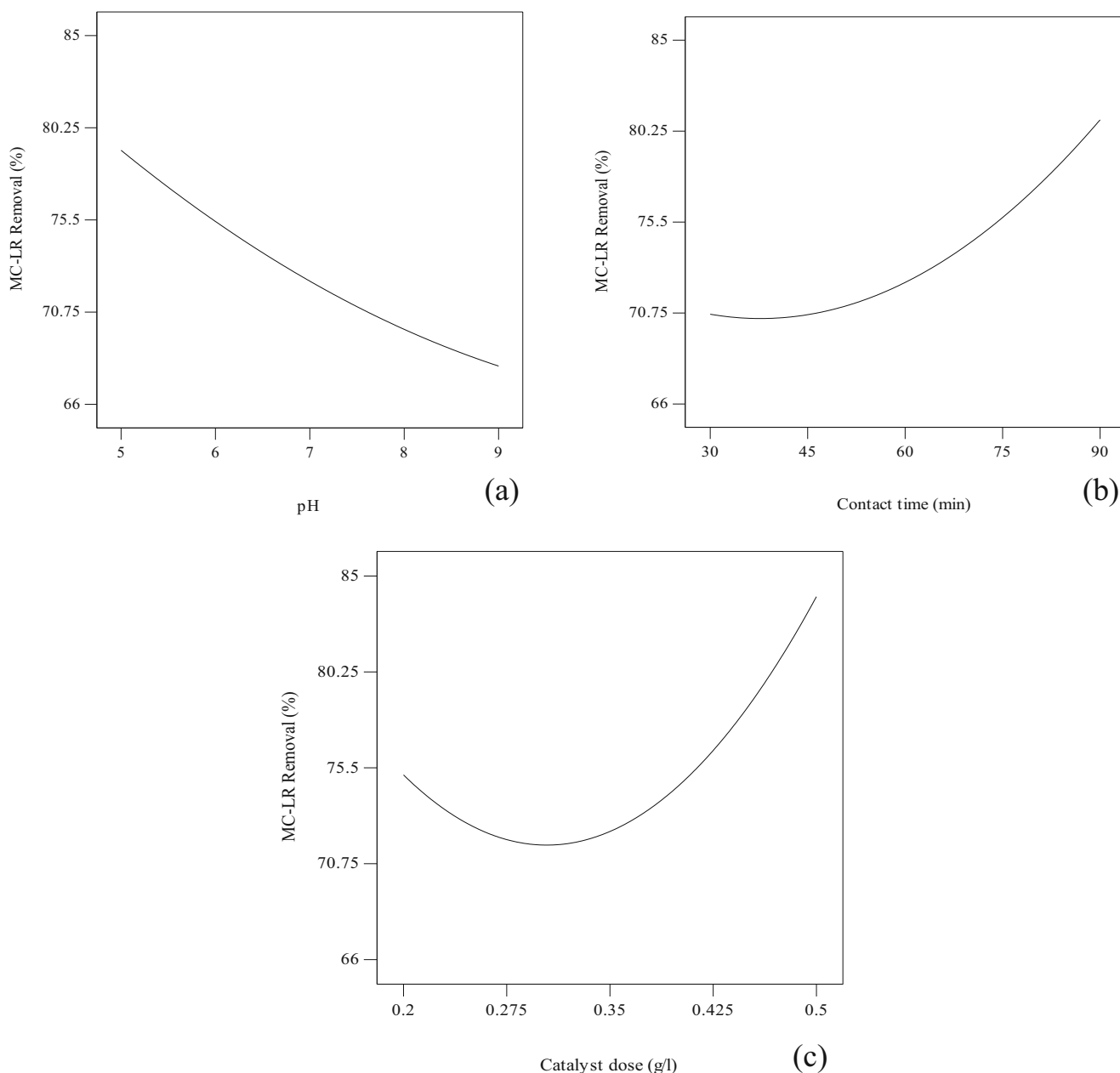
Fig. 5 Effect of pH (A), contact time (B) and catalyst dose (C) on MC-LR degradation (%)

forming between these molecules and photocatalysts surface [52].

2) Hydrophobic characteristic of the MC-LR due to being a large molecule (MW = 995 g/mol) and having the complex of amino acids [52]. So that, Lawton et al. reported that hydrophobicity was the most important factor controlling the adsorption of MCs on the surface of TiO_2 catalysts [53]. Also, Chen et al. observed that the hydrophobic property of the Adda group in MCs helps its sorption on the surface of Bi_2WO_6 nanoparticles [54].

3) The increasing of MC-LR solubility in water that leads to the reaction of between the MC-LR and catalysts through the ion pairing effect [55].

4) The formation of •H radicals. According to Liu et al. study, solution pH has an important effect on MC-LR removal, so that when pH was in the acidic conditions, a better removal rate by·•H radicals was found, due to the main path of MC-LR degradation and Adda strain removal [56].

Effect of contact time

The contact time has a positive effect on MC-LR removal. On the other word, the removal efficiency of MC-LR was enhanced with increasing contact time in the range of 30 to

90 min (Fig. 5B). Because of increasing contact time enhances the reaction time between the MC-LR and photocatalysts and then its effective removal [57]. Zhang et al. showed that the removal efficiency of the MC-LR increased over the time [55]. In Nasseri et al. study, Malathion adsorption and photocatalytic removal were increased with enhancing of contact time [47]. Similar results reported by Mortazavian et al., that increasing reaction time improved removal percentages for dyes [50].

Effect of catalyst dose

Figure 5C shows the effect of catalyst dose on MC-LR degradation. The removal efficiency of MC-LR is increased with increasing catalyst dose in the range of 0.2 to 0.5 g/l. Zhang et al. reported that the removal efficiency of MC-LR was improved with an increase in catalyst dosage because of the surface area of the catalysts increased with increasing dosage. Therefore, the selection of the optimum catalyst dose was important with consideration of its cost and effects [55]. Also, Mortazavian et al. reported that the increasing catalyst dose, enhanced photocatalytic degradation efficiencies of textile dyes [50].

Interaction between variables

Figure 6a shows the interaction between pH and contact time as a 2-dimensional graph. According to this figure, the MC-LR removal efficiency was increased by increasing of contact time and decreasing of pH. Of course, the coefficient of this term in Eq. 10 is less than the coefficient of each variable.

Figure 6b illustrates the interaction between pH and catalyst dosage. In this Figure, it can be seen by pH reduction and increasing of catalyst dose, the MC-LR removal efficiency

was increased. However, the model coefficient of this term in Eq. 10 is lower than each of the variables only.

Optimization the process and model verification

The aim of this study was to determine the optimum amount of parameters with the RSM model which lead to the highest MC-LR removal efficiency. In this regard, the optimization of influencing variables was necessary. The desirable goal in MC-LR degradation was set on the maximum value. The synthesized BiVO$_4$ nanoparticles had highest MC-LR removal efficiency about 93% at these conditions: pH = 5, contact time = 180 min and catalyst dose = 0.5 g/l. While, purchased TiO$_2$ nanoparticles in the best conditions (pH = 5, contact time = 30 min and catalyst dose = 1 g/l) had about 95% MC-LR removal efficiency. The prepared nanocomposite BiVO$_4$/TiO$_2$ showed extremely enhanced photocatalysis characteristics compared to the individual BiVO$_4$ and TiO$_2$ [58]. So that, the highest MC-LR removal efficiency (about 98%) by the BiVO$_4$/TiO$_2$ nanocomposite was obtained at the optimum conditions: pH = 5, contact time = 90 min and catalyst dose = 0.5 g/l. Therefore, synergetic effect of the porous nanostructures can enhance the photocatalytic activity of nanocomposite photocatalysts [59]. Ultimately, in order to estimate the validity of these optimal conditions, a series of MC-LR removal experiments were implemented which their results were in good accordance with Design Expert predictions.

Conclusions

Microcystins cause poisoning for livestock and wildlife and also pose a health hazard for humans through of the drinking water. The removal of these pollutants from water sources is
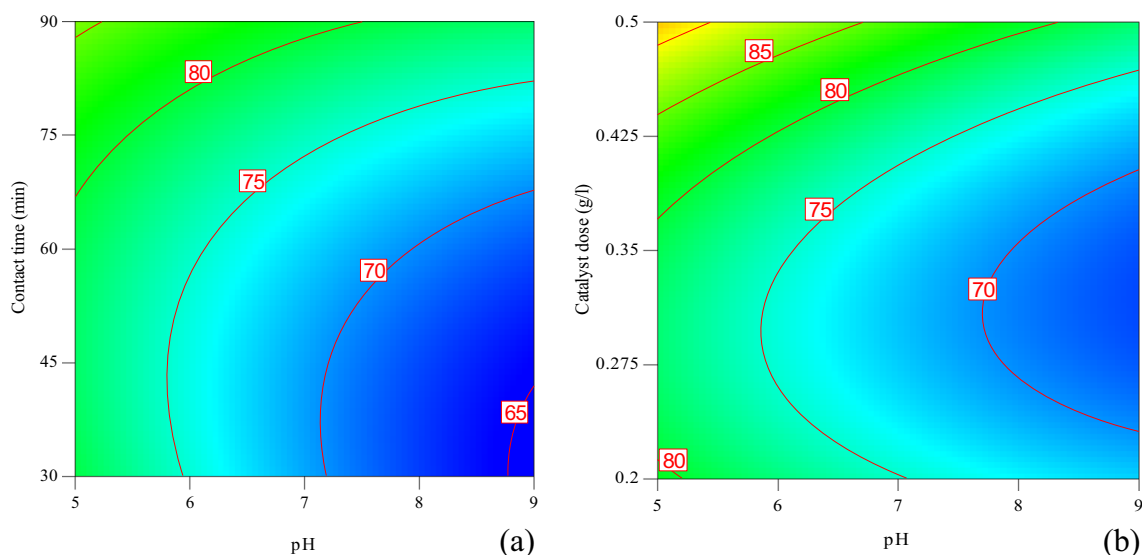

Fig. 6 2-dimensional graph of interaction between variable of pH with contact time (a) and catalyst dose (b) in the MC-LR removal (%)

done by various techniques, each one with its own advantages and disadvantages. Photocatalytic degradation is one of the methods for water purification developed in recent years. According to the results, use of $BiVO_4/TiO_2$ nanocomposite can greatly improve removal efficiency of these compounds. In the present study; the effect of important parameters such as pH, contact time, and catalyst dose on MC-LR removal were evaluated using RSM technique based on CCD design. The results showed that the optimum conditions for MC-LR removal by the $BiVO_4/TiO_2$ nanocomposite were pH = 5, contact time = 90 min, and catalyst dose = 0.5 g/l. Under these circumstances, MC-LR removal efficiency was about 98%. Based on the analysis results of FESEM, XRD, and FTIR; it was found that the materials used in the photocatalytic process had been correctly identified. Therefore, In this study $BiVO_4/TiO_2$ nanocomposite was approved as a promising nano-photocatalyst for MC-LR removal. Experimental design is an effective method for reducing experiments and costs that can help in better understanding of the effect of independent variables on response.

Compliance with ethical standards

Conflict of interest   Authors declare in this study has no conflict of interest.

References

1. Liu L, Huang Q, Qin B. Characteristics and roles of Microcystis extracellular polymeric substances (EPS) in cyanobacterial blooms: a short review. J Freshw Ecol. 2018;33(1):183–93.
2. Shamsollahi HR, Alimohammadi M, Nabizadeh R, Nazmara S, Mahvi AH. Monitoring of microcystin-LR concentration in water reservoir. Desalin Water Treat. 2018;126:345–9.
3. Sharma VK, Chen L, Marsalek B, Zboril R, O'Shea KE, Dionysiou DD. Iron based sustainable greener technologies to treat cyanobacteria and microcystin-LR in water. Water Sci Tech-W Sup. 2016;17(1):107–14.
4. Sorlini S, Gialdini F, Collivignarelli C. Removal of cyanobacterial cells and microcystin-LR from drinking water using a hollow fiber microfiltration pilot plant. Desalination. 2013;309:106–12.
5. Jaša L, Sadílek J, Kohoutek J, Straková L, Maršálek B, Babica P. Application of passive sampling for sensitive time-integrative monitoring of cyanobacterial toxins microcystins in drinking water treatment plants. Water Res. 2019;153:108–20.
6. Campos A, Vasconcelos V. Molecular mechanisms of microcystin toxicity in animal cells. Int J Mol Sci. 2010;11(1):268–87.
7. Shamsollahi HR, Alimohammadi M, Nabizadeh R, Nazmara S, Mahvi AH. Measurement of microcystin-LR in water samples using improved HPLC method. Glob J Health Sci. 2015;7(2):66.
8. Janssen EM-L. Cyanobacterial peptides beyond microcystins–a review on co-occurrence, toxicity, and challenges for risk assessment. Water Res. 2019;151:488–99.
9. Antoniou MG, De La Cruz AA, Dionysiou DD. Cyanotoxins: New generation of water contaminants. J Environ Eng-ASCE. 2005;131:9.
10. Yan H, Gong A, He H, Zhou J, Wei Y, Lv L. Adsorption of microcystins by carbon nanotubes. Chemosphere. 2006;62(1):142–148.11.
11. Liu B, Qu F, Chen W, Liang H, Wang T, Cheng X, et al. Microcystis aeruginosa-laden water treatment using enhanced coagulation by persulfate/Fe (II), ozone and permanganate: comparison of the simultaneous and successive oxidant dosing strategy. Water Res. 2017;125:72–80.
12. Mokoena M, Mukhola M, Okonkwo O. Hazard assessment of microcystins from the household's drinking water. Appl Ecol Env Res. 2016;14(3):695–710.13.
13. Pham T-L, Dang TN. Microcystins in freshwater ecosystems: occurrence, distribution, and current treatment approaches. Water and Wastewater Treatment Technologies: Springer; 2019: 15–36.
14. Roegner AF, Brena B, González-Sapienza G, Puschner B. Microcystins in potable surface waters: toxic effects and removal strategies. J Appl Toxicol. 2014;34(5):441–57.
15. Fan J, Ho L, Hobson P, Brookes J. Evaluating the effectiveness of copper sulphate, chlorine, potassium permanganate, hydrogen peroxide and ozone on cyanobacterial cell integrity. Water Res. 2013;47(14):5153–64.
16. Fan W, Zhang Q, Wang Y. Semiconductor-based nanocomposites for photocatalytic H_2 production and CO_2 conversion. Phys Chem Chem Phys. 2013;15(8):2632–49.
17. Pantelić D, Svirčev Z, Simeunović J, Vidović M, Trajković I. Cyanotoxins: characteristics, production and degradation routes in drinking water treatment with reference to the situation in Serbia. Chemosphere. 2013;91(4):421–41.
18. Liu Y, Ren J, Wang X, Fan Z. Mechanism and reaction pathways for microcystin-LR degradation through UV/H_2O_2 treatment. PLoS One. 2016;11(6):e0156236.
19. Karci A, Wurtzler EM, Armah A, Wendell D, Dionysiou DD. Solar photo-Fenton treatment of microcystin-LR in aqueous environment: transformation products and toxicity in different water matrices. J Hazard Mater. 2018;349:282–92.
20. Park J-A, Yang B, Park C, Choi J-W, van Genuchten CM, Lee S-H. Oxidation of microcystin-LR by the Fenton process: kinetics, degradation intermediates, water quality and toxicity assessment. Chem Eng. 2017;309:339–48.
21. Pinho LX, Azevedo J, Brito Â, Santos A, Tamagnini P, Vilar VJ, et al. Effect of TiO_2 photocatalysis on the destruction of Microcystis aeruginosa cells and degradation of cyanotoxins microcystin-LR and cylindrospermopsin. Chem Eng. 2015;268:144–52.
22. Miao H-F, Qin F, Tao G-J, Tao W-Y, Ruan W-Q. Detoxification and degradation of microcystin-LR and -RR by ozonation. Chemosphere. 2010;79(4):355–61.
23. Song W, De La Cruz AA, Rein K, O'Shea KE. Ultrasonically induced degradation of microcystin-LR and -RR: identification of products, effect of pH, formation and destruction of peroxides. Environ. Sci. Technol. 2006;40(12):3941–6.
24. Zong W, Sun F, Sun X. Oxidation by-products formation of microcystin-LR exposed to UV/H_2O_2: toward the generative mechanism and biological toxicity. Water Res. 2013;47(9):3211–9.
25. Kabra K, Chaudhary R, Sawhney RL. Treatment of hazardous organic and inorganic compounds through aqueous-phase photocatalysis: a review. Ind Eng Chem Res. 2004;43(24):7683–96.

26. Baiju K, Shukla S, Sandhya K, James J, Warrier K. Photocatalytic activity of sol− gel-derived nanocrystalline titania. J Phys Chem C. 2007;111(21):7612–22.

27. Choi H, Sofranko AC, Dionysiou DD. Nanocrystalline TiO2 photocatalytic membranes with a hierarchical mesoporous multilayer structure: synthesis, characterization, and multifunction. Adv Funct Mater. 2006;16(8):1067–74.

28. Hirakawa T, Sato K, Komano A, Kishi S, Nishimoto CK, Mera N, et al. Experimental study on adsorption and photocatalytic decomposition of isopropyl methylphosphonofluoridate at surface of TiO2 photocatalyst. J Phys Chem C. 2010;114(5):2305–14.

29. Pal S, Laera AM, Licciulli A, Catalano M, Taurino A. Biphase TiO2 microspheres with enhanced photocatalytic activity. Ind Eng Chem Res. 2014;53(19):7931–8.

30. Golmojdeh H, Zanjanchi M. A facile approach for synthesis of BiVO4 nanoparticles possessing high surface area and various morphologies. Cryst Res Technol. 2012;47(9):1014–25.

31. Kumar SG, Devi LG. Review on modified TiO2 photocatalysis under UV/visible light: selected results and related mechanisms on interfacial charge carrier transfer dynamics. J Phys Chem A. 2011;115(46):13211–41.

32. Sun J, Li X, Zhao Q, Ke J, Zhang D. Novel V2O5/BiVO4/TiO2 nanocomposites with high visible-light-induced photocatalytic activity for the degradation of toluene. J Phys Chem C. 2014;118(19):10113–21.

33. Seabold JA, Choi K-S. Efficient and stable photo-oxidation of water by a bismuth vanadate photoanode coupled with an iron oxyhydroxide oxygen evolution catalyst. J Am Chem Soc. 2012;134(4):2186–92.

34. Zhou D, Pang L-X, Guo J, Wang H, Yao X, Randall C. Phase evolution, phase transition, Raman spectra, infrared spectra, and microwave dielectric properties of low temperature firing (K0.5xBi1−0.5x)(MoxV1−x)O4 ceramics with Scheelite related structure. Inorg Chem. 2011;50(24):12733–8.

35. Wetchakun N, Chainet S, Phanichphant S, Wetchakun K. Efficient photocatalytic degradation of methylene blue over BiVO4/TiO2 nanocomposites. Ceram Int. 2015;41(4):5999–6004.

36. Aslani H, Nabizadeh R, Nasseri S, Mesdaghinia A, Alimohammadi M, Mahvi AH, et al. Application of response surface methodology for modeling and optimization of trichloroacetic acid and turbidity removal using potassium ferrate (VI). Desalin Water Treat. 2016;57(52):25317–28.

37. Bussi J, Ohanian M, Vázquez M, Dalchiele EA. Photocatalytic removal of hg from solid wastes of chlor-alkali plant. J Environ Eng. 2002;128(8):733–739.38.

38. Huang H, Xiao K, He Y, Zhang T, Dong F, Du X, et al. In situ assembly of BiOI@ Bi12O17Cl2 pn junction: charge induced unique front-lateral surfaces coupling heterostructure with high exposure of BiOI {001} active facets for robust and nonselective photocatalysis. Appl Catal B-Environ. 2016;199:75–86.

39. Huang H, He Y, Li X, Li M, Zeng C, Dong F, et al. Bi2O2(OH)(NO3) as a desirable [Bi2O2]2+ layered photocatalyst: strong intrinsic polarity, rational band structure and {001} active facets co-beneficial for robust photooxidation capability. J Mater Chem A. 2015;3(48):24547–56.

40. Huang H, Li X, Wang J, Dong F, Chu PK, Zhang T, et al. Anionic group self-doping as a promising strategy: band-gap engineering and multi-functional applications of high-performance CO32− doped Bi2O2CO3. ACS Catal. 2015;5(7):4094–103.

41. Rajalingam V. Synthesis and characterization of BiVO4 nanostructured materials: application to photocatalysis: Université du Maine; 2014.

42. Matthiensen A, Beattie KA, Yunes JS, Kaya K, Codd GA. [D-Leu1] microcystin-LR, from the cyanobacterium Microcystis RST 9501 and from a Microcystis bloom in the Patos lagoon estuary, Brazil. Phytochemistry. 2000;55(5):383–7.

43. Hu Y, Chen W, Fu J, Ba M, Sun F, Zhang P, et al. Hydrothermal synthesis of BiVO4/TiO2 composites and their application for degradation of gaseous benzene under visible light irradiation. Appl Surf Sci. 2018;436:319–26.

44. Rahimi B, Ebrahimi A. Photocatalytic process for total arsenic removal using an innovative BiVO4/TiO2/LED system from aqueous solution: optimization by response surface methodology (RSM). J Taiwan Inst Chem E. 2019;101:64–79.

45. Mohammadi A, Nemati S, Mosaferi M, Abdollahnejhad A, Almasian M, Sheikhmohammadi A. Predicting the capability of carboxymethyl cellulose-stabilized iron nanoparticles for the remediation of arsenite from water using the response surface methodology (RSM) model: modeling and optimization. J Contam Hydrol. 2017;203:85–92.

46. Venkatachalam N, Palanichamy M, Murugesan V. Sol–gel preparation and characterization of alkaline earth metal doped nano TiO2: efficient photocatalytic degradation of 4-chlorophenol. J Mol Catal A-Chem. 2007;273(1–2):177–85.

47. Nasseri S, Borna MO, Esrafili A, Kalantary RR, Kakavandi B, Sillanpää M, et al. Photocatalytic degradation of malathion using Zn2+−doped TiO2 nanoparticles: statistical analysis and optimization of operating parameters. Appl Phys A Mater Sci Process. 2018;124(2):175.

48. Bhatkhande DS, Pangarkar VG, Beenackers AA. Photocatalytic degradation for environmental applications–a review. J ChemTechnol Biotechnol. 2002;77(1):102–16.

49. He X, Pelaez M, Westrick JA, O'Shea KE, Hiskia A, Triantis T, et al. Efficient removal of microcystin-LR by UV-C/H2O2 in synthetic and natural water samples. Water Res. 2012;46(5):1501–10.

50. Mortazavian S, Saber A, James DE. Optimization of Photocatalytic degradation of acid blue 113 and acid red 88 textile dyes in a UV-C/TiO2 suspension system: application of response surface methodology (RSM). Catalysts. 2019;9(4):360.51.

51. Rahimi B, Jafari N, Abdolahnejad A, Farrokhzadeh H, Ebrahimi A. Application of efficient photocatalytic process using a novel BiVO/TiO2-NaY zeolite composite for removal of acid orange 10 dye in aqueous solutions: modeling by response surface methodology (RSM). J Environ Chem Eng. 2019;7(4):103253.

52. Huang W-J, Cheng B-L, Cheng Y-L. Adsorption of microcystin-LR by three types of activated carbon. J Hazard Mater. 2007;141(1):115–22.

53. Lawton LA, Robertson PK, Cornish BJ, Marr IL, Jaspars M. Processes influencing surface interaction and photocatalytic destruction of microcystins on titanium dioxide photocatalysts. J Catal. 2003;213(1):109–13.

54. Chen P, Zhu L, Fang S, Wang C, Shan G. Photocatalytic degradation efficiency and mechanism of microcystin-RR by mesoporous Bi2WO6 under near ultraviolet light. Environ Sci Technol. 2012;46(4):2345–51.

55. Zhang H, Zhu G, Jia X, Ding Y, Zhang M, Gao Q, et al. Removal of microcystin-LR from drinking water using a bamboo-based charcoal adsorbent modified with chitosan. J Environ Sci. 2011;23(12):1983–8.

56. Liu S, Hu X, Jiang W, Ma L, Cai M, Xu H, et al. Degradation of microcystins from Microcystis aeruginosa by 185-nm UV irradiation. Water Air Soil Pollut. 2016;227(4):129.

57. Pavithra KG, Kumar PS, Christopher FC, Saravanan A. Removal of toxic Cr (VI) ions from tannery industrial wastewater using a newly designed three-phase three-dimensional electrode reactor. J Phys Chem Solids. 2017;110:379–85.

58. Huang H, He Y, Du X, Chu PK, Zhang Y. A general and facile approach to heterostructured core/shell BiVO$_4$/BiOI p–n junction: room-temperature in situ assembly and highly boosted visible-light photocatalysis. ACS Sustain Chem Eng. 2015;3(12):3262–73.

59. Huang H, Xiao K, Zhang T, Dong F, Zhang Y. Rational design on 3D hierarchical bismuth oxyiodides via in situ self-template phase transformation and phase-junction construction for optimizing photocatalysis against diverse contaminants. Appl Catal B-Environ. 2017;203:879–88.